Non-destructive Material Investigation with Thermal Neutrons at the TRIGA Mark II Reactor in Vienna

M. Bastürk, H. Böck, B. Zamani, M. Zawisky, H. Rauch
Atomic Institute of the Austrian Universities, Stadionallee 2, A-1020 Vienna, Austria

Abstract: Neutron tomography providing 3D information about interior of an object is a very efficient tool to visualize inner defects of the materials, non-destructively. In this study, some applications of neutron tomography in different fields such as geology, aerospace, civil engineering and archaeology were presented. Distribution of minerals in pumice and rock samples, visualization of inner defects within a new developed titan aluminum turbine blade, and distribution of silica gel as an important impregnating agent in construction and restoration of buildings were investigated. The measurements of tomography projections taken in the 0 to 180° angle were performed with a thermal neutron flux of 10^5 at the TRIGA Mark II research reactor in Vienna, and the common Filtered Back Projection method was used for the 3D image reconstruction.

1 Introduction

The neutron radiography is a very efficient tool to investigate materials non-destructively. It can be grouped into three categories depending on its energy spectrum: cold-, thermal- and fast neutron radiography. The principle of neutron radiography is based on the attenuation of the neutron beam by the materials and a consequently detection of the transmitted neutron beam with a position sensitive detector such as converter/film or scintillator/digital camera system. In this way due to the differences in intensity (attenuation of the neutron beam by the matter), the inner structure of materials can be visualized. In contrary to X-rays, which interact with the electron shell of the atoms, neutrons interact with their nucleus. Therefore, discrimination between different isotopes is possible. Important parameters for the imaging quality are the beam collimation (L/D ratio), high neutron flux and low background. A beam with a high collimation ratio improves significant the image sharpness [1].

Neutron tomography gives detailed information about the inner structure of the object from a set of projections. 2D projections are conventional radiography images, and in order to collect the whole number of projections step by step in an angular interval (0° - 180°), the sample is placed on a rotary table in front of the position sensitive detector. Experimental data are preprocessed with image processing routines and then reconstructed by reconstruction software.

ATI-Vienna has two NR beam ports (NR-I, NR-II); NR-I based on neutron converter/X-rays film is used for radiographic inspections of large objects, and NR-II having a digital detection system (neutron sensitive scintillator/digital CCD camera) is for radiographic and tomographic applications [2,3]. In a digital detection system, the transmitted neutrons are absorbed in a neutron sensitive scintillator where they are converted to photons detected finally by a CCD camera. The scintillator should have a high absorption cross section for thermal neutrons, a high light output per absorbed neutron and low gamma sensitivity [2]. The spatial image resolution determined by using a thin Gd-foil is between 180 to 500 μm for the NR II described above. The 3D image reconstruction program based on the common filtered back projection method was developed at the Atominstitute-Vienna using IDL 5.3 software. The related theory concerning the reconstruction can be found in detail in [1,2]. The main characteristics of our NR set-ups and at the ATI-Vienna and their comparison with the

NEUTRA facility at PSI where some of the measurements presented in this paper were carried out are given in Table-I.

Table-I: Characteristics of the NR beam ports at ATI and PSI.

	NR-I (ATI)	NR-II (ATI)	NEUTRA (PSI)
Neutron flux ($cm^{-2}.s^{-1}$)	$3x10^5$	$1.3x10^5$	$3x10^6$
Collimation ratio	50	130	550
Cd ratio	3	20	100
Beam diameter (cm)	40	9	40
Detection system	Gd converter/ X-ray film	0.4 mm thick ZnS(Ag)-^{6}LiF scintillator/CCD camera (512x512 pixels)	0.25 mm thick ZnSAg-^{6}LiF scintillator/CCD camera (1024x1024 pixels)

2 Applications of Neutron Tomography

2.1 NT Application in Nuclear Technology: First wall & Structural material in Fusion Reactors and study of boron alloyed steels (shielding material)

A fiber reinforced silicon carbide ceramic composite (SiC/SiC_f), developed by CERACEP® has been studied as a structural and an alternative first wall material for blanket concept in fusion reactors. Despite the increased shielding requirements (low attenuation cross section of SiC), the use of SiC/SiC is economically justified due to the high thermal efficiency, which may reduce the cost of electricity by 15 %. In spite of the CVI method producing low porosity materials, the porosity remains a problem in ceramic composites. The maximum thickness of the SiC/SiC_f structural material considering the porosity problem is about 6 mm. Nevertheless, the required thickness for the TAURO blanket concept is between 10–15 mm. The porosity within the composites causes a reduction of the thermal conductivity as well as a limitation of the material thickness in the production process [4,5]. For this reason, the investigation of the defects and porosities in the structural material is very important.

According to the thermal NR images given in Fig. 1, the 3 mm thick N3-1 SiC/SiC_f sample seems to be very homogeneous and also free of porosity and defects with our detection systems. On the other hand, X-rays radiography delivered some details about the texture of a 3 mm thick SiC/SiC_f composite, which attenuates X-Rays more than thermal neutrons. In addition, N3-1 SiC/SiC_f samples were inspected with low energy neutrons at PSI. The main reason for the imaging with cold neutrons (Energy Selective Neutron Radiography and Tomography-ESNR&ESNT) is the enhancement of the contrast from the abrupt change of the neutron attenuation properties of solids at Bragg cut-off energies. The porosity distribution within the fiber bundles was visualized by neutron radiography measurements at a 3 mm thickness of N3-1 SiC/SiC_f sample (where 3 mm is much smaller than the maximum producible thickness of 6 mm). As a detection system for these measurements, a 12-bit CCD camera having 1280x1024 pixels and 6.7x6.7 μm pixel size with a 0.1 mm thick Levy Hill neutron scintillator was used [4,5]. The ESNT measurement was performed in order to provide 3D information on the inner sample structure.

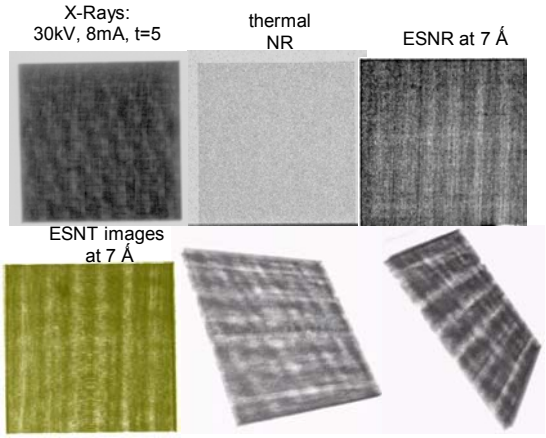

Fig.1: The radiography and tomography images of the N3-1 SiC/SiC$_f$ ceramic composite (2x2x0.3 cm^3 size) taken by X-Rays, thermal NR, cold NR/NT at 7 Å neutron wavelength.

Additionally, a 8 mm thick SiC/SiC$_f$ composite bonded on 2 mm thick Cu metal was visualized with neutron and X-Rays imaging methods. Owing to the high X-Rays attenuation of such a thick sample, we could not get any image contrast. On the other hand, thermal NR&NT and ESNR images show a distribution of fiber bundles-alignment in one direction (Fig. 2).

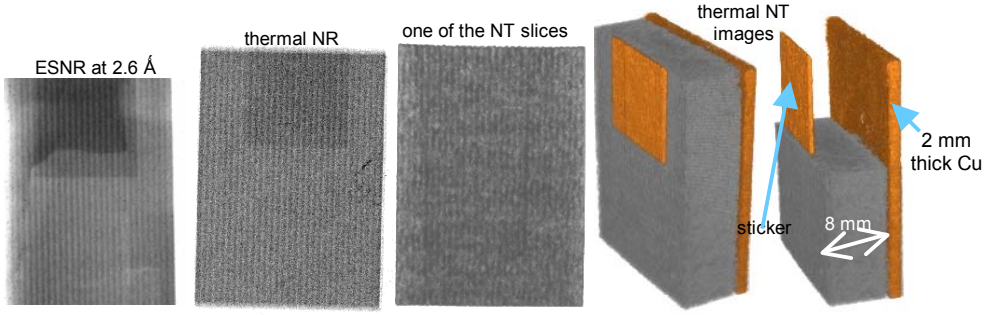

Fig.2: The fiber bundle alignment in one direction within the bonded SiC/SiC$_f$ composite with a size of 2 cm x 3 cm x 1 cm observed even with thermal neutron radiography for thicker composites.

Boron alloyed steel sheets are used in nuclear engineering as neutron shielding for radioactive waste disposal equipment, such as components for compact fuel storage racks and transportation baskets. The main demand on the sheets and plates for these applications is the largest possible thermal neutron attenuation, which has to be uniform over the volume [6,7]. The ^{10}B isotope has a large attenuation cross section for thermal neutrons ($\sigma_{th}(^{10}B)$ = 3838.1(10)×10^{-24} cm^2) [8]. The natural abundance of ^{10}B is 18.85 wt% therefore boron enriched with ^{10}B can considerably increase the neutron absorption and reduce the weight of neutron shielding. The transmission analysis with thermal neutrons is of particular interest because it yields a realistic shielding factor of the steels, e.g., for the compact fuel storage in water.

The transmission analysis can be performed with high spatial resolution in the order of 0.1 mm and is, contrary to mass spectroscopy, very sensitive to absorber inhomogeneities and geometrical defects in the whole illuminated volume. In the investigation of thick steels we found pronounced deviations from the exponential attenuation law (Fig. 3), mainly caused by the beam hardening effect [9,10]. The beam hardening increases with the macroscopic cross section, the thickness and the spectral width.

Micro-heterogeneities of the ferro-borides in the steel have been identified as another source of the enhanced neutron transmission [10]. Secondary factors, the beam hardening and

inhomogeneity cause an elevation of the effective neutron transmission through the material which has to be considered in the design of neutron shielding.

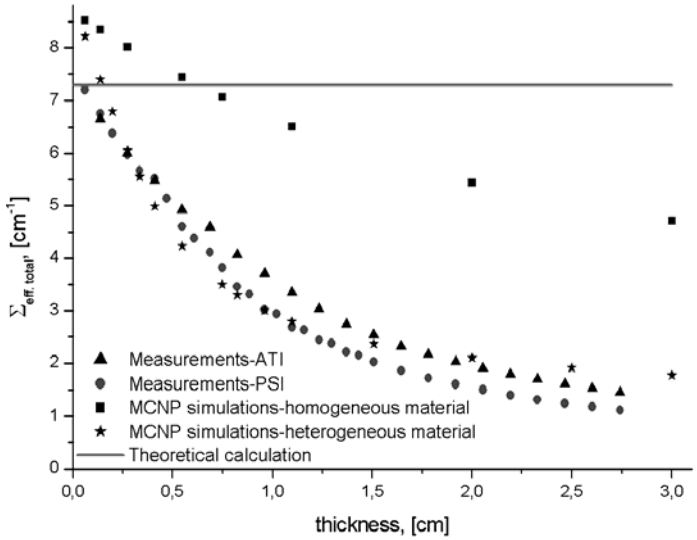

Fig.3: Neutron attenuation by natural boron-alloyed steel plates showing a deviation from the exponential attenuation law due to the beam hardening and other factors like background, micro-heterogeneous structure.

The production of ^{10}B enriched steels is rather expensive, therefore all possible sources of systematic inhomogeneities during the production process (melting, welding, milling, cutting) must be excluded from a complete three-dimensional absorber analysis. Within the steel project, a set of boron alloyed steel rods with different ^{10}B enrichment was bored out of thick steel sheets at different locations. Tomographic volume inspections can also be performed on small reactor sources like the 250 kW TRIGA reactor, because within the thermal spectrum the neutrons with higher energies penetrate even thick and strong absorbing materials. But the tomographic analysis requires a low background level and a careful correction of the beam hardening artifact [11]. The spatial resolution lies between 200 – 400 μm, depending on the sample – scintillator distance. The typical exposure time for one projection is 2 min and we chose about 60 projections for a strong absorbing rod. Fig. 4 shows the reconstruction of the effective (left) and thermal (right) total macroscopic cross-sections of a highly ^{10}B enriched steel rod. After the beam hardening correction a uniform distribution of the ^{10}B isotopes was confirmed.

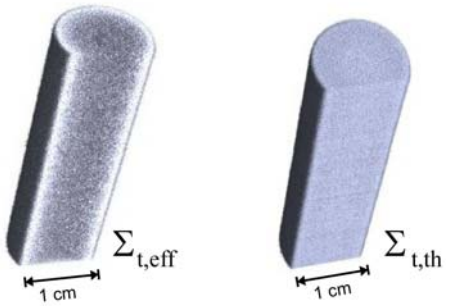

Fig.4: 3D rendering of a highly enriched (^{10}B/B = 97.4 at%) boron alloyed steel rod with 1 cm diameter ($\Sigma_{t,th}$ = 12.7 cm^{-1}). Left: Variation of the effective cross-sections. Right: Beam hardening correction yields a uniform distribution of thermal cross-sections [11].

The corrected reconstruction (right) yields a rather homogeneous profile, which has independently been verified by neutron radiography and chemical analysis. The macroscopic thermal cross section ($\Sigma_{t,th}$) relates to the density of the ^{10}B isotope in the steel as in Eq.(1).

$$\rho(^{10}B) = \frac{M(^{10}B)\Sigma_{th}(^{10}B)}{N_A\,\sigma_{th}(^{10}B)} \qquad \text{(Eq.1)}$$

The atomic weight, $M(^{10}B)$ = 10.0129g, the Avogadro constant, N_A = 6.02214199(47)x10^{23} mol^{-1}, and the microscopic cross-section $\sigma_{th}(^{10}B)$, are known with high accuracy. Hitherto, we applied the tomographic technique primarily to our steel samples, but the macroscopic cross section of uranium fuel elements lies within the range of the absorbing steels. The presented tomographic technique can therefore also be employed in the non-destructive inspection of fuel elements, and this can be achieved with rather weak neutron sources.

2.2 NT Application in Aerospace

This study aimed to visualize manufacturing defects or inner cracks for quality control of a new turbine blade material [47Ti-48Al-2Cr-2Nb-1B (atom %)] resulting from the manufacturing process. At the beginning, neutron and X-ray radiography measurements of the TiAl test sample developed by the Institute of Physics of Materials in Czech Republic were performed at Atominstitut in order to find the most efficient method. Excellent properties at elevated-temperatures and low density make the titanium aluminide (TiAl) an attractive candidate for both, engine and airframe applications, particularly in the aerospace industry. Among TiAl-based materials, gamma TiAl is the most promising alternative. It reduces the weight of aircraft engines by virtue of its low density and high temperature capability, and has advantages in stiffness, fire and corrosion resistance. The performance in the transitional state between the turbine at rest and a particular speed of rotation is important in order to improve the efficiency. The use of light materials such as gamma TiAl alloy for the turbine blades is desirable in reducing the transitional time and inertia of the turbine rotors. The characteristics of aircraft engines affect the revenue, as well as the total weight reduction [12,13,14]. The addition of the elements Cr and B increases the room temperature ductility, and Nb the oxidation resistance. Boron forms TiB_2 borides, which improve the stability of the grain structures during various thermo-mechanical treatments. The mechanism of ductilization is unclear; it is assumed that the boron segregates into grain boundaries, enhancing thus the cohesive strength of the boundary [15,16]. Hence, prototype TiAl turbine blades containing 1 at% B were investigated. In addition to the material characteristics, aero-engine applications require careful processing route involving casting, forging, machining or joining to produce complex geometries. The final mechanical properties of the alloy depend strongly on the machining [16,17].

According to the X-ray image taken at 55 kV, 20 mA for 60 s exposure time gave insufficient information about the TiAl turbine blade; the thickness of turbine blade varies from 2 mm to ~ 2 cm. As a result, an increase in energy and density of X-rays beam caused disappearance of the image contrast in thinner parts of the sample. On the other hand, the sample is quite transparent for neutrons. Neutron tomography was applied in order to get more information about the sample's interior. For 3D image reconstruction, 200 NR projections were taken with 40 s exposure time per projection with 0.9° angular steps from different views. Enhancing the image contrast and cutting the 3D images slice by slice with the help of the rendering software (VolumeGraphics), the inhomogeneities and defects within the sample were visualized in Fig. 5 (marked parts). The inhomogeneity increases with the thickness of the turbine blade. In addition, some defects like cracks that might form during the material processing (casting, forging, machining and joining) could be visualized as marked in Fig. 5. No further inhomogeneity respective to the distribution of boron (1 at%) was detected within the spatial resolution of 300 μm.

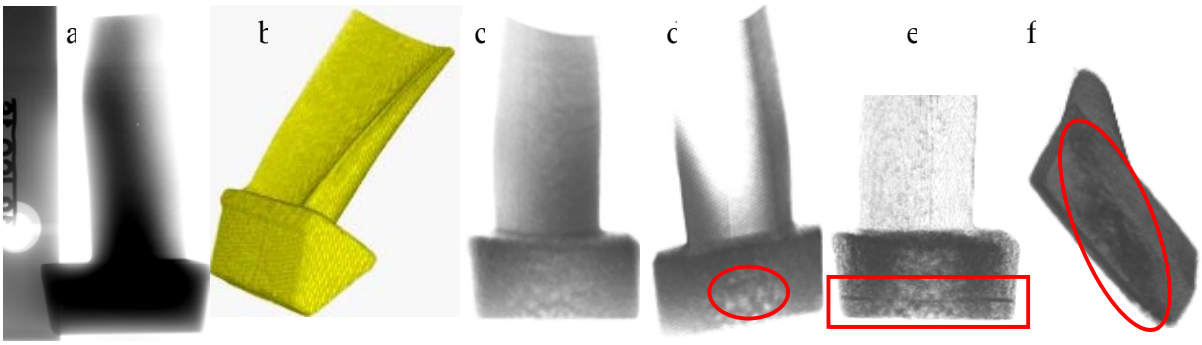

Fig.5: X-Rays radiography (fig.5a) and 3D reconstructed NT images of the TiAl turbine blade with different opacity levels; the inhomogeneous parts were marked, fig.5b and 5f are with full opacity, fig.5c, -d, -e with enhanced contrast. Fig. 5e with high transparency shows a crack or defect in the middle of the sample.

2.3 Application in Geology/Mineralogy

Another application of neutron radiography (NR) and neutron tomography (NT) presented in this work helps to visualize the distribution of minerals in rocks. Size and distribution of minerals as well as the internal structure yield valuable information for petrologic research and for the applicability as construction material. Example is the distribution of mica in volcanic pumice. The NT measurements were performed at the PSI with ~ 100 µm spatial resolution. The volcanic pumice, a highly vesicular volcanic rock, mainly consists of silicate glass. The mineral biotite (black mica) contains significantly more iron and hydrogen than the surrounding glass and is well shown due to the higher neutron absorption cross sections of these elements (Fig. 6). To facilitate the visualization of biotite, a segmentation process was applied; the yellow colored parts indicate biotite while the gray colored parts are silicate glass. Furthermore, one of the segments (in this case glass) was cut to highlight the other segment. The mineral biotite is shown while the other mineral components such as quartz and feldspar show properties similar to that of the pumice glass.

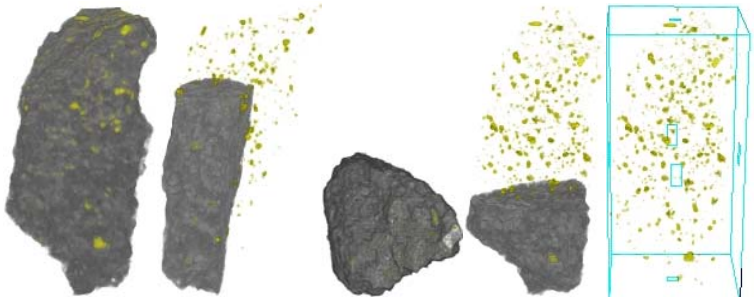

Fig.6: 3D reconstructed NT images of pumice from different views (240 projections taken with 10 seconds exposure time each), which show two segments indicating pumice (grey) and biotite (yellow, the pumice segment was cut slice by slice to highlight the biotite segment in the last image).

2.4 Application in Civil Engineering

Silica gel (SiO_2) is an important impregnation agent for the preservation of natural stone surfaces of historical buildings to prevent progressive weathering [18]. The surfaces are impregnated with a solution of tetraethoxysilane, which decomposes by precipitation of silica gel and evaporation of ethanol. Silica gel adsorbs the water and retains in itself, which offers good properties for a 3D imaging by NT. The quality of an impregnation depends on the distribution of the agent throughout the (usually porous) rock structure and can therefore be

checked by NT. Additionally, the quantity necessary can be optimized economically. As an example, an impregnated sample of tertiary calcareous sandstone (St. Margarethen, Austria) was investigated. The material has been prepared during a research cooperation for the restoration of St. Stephen's cathedral in Vienna, Austria. The measurements performed at ATI improved our understanding of the water adsorption by silica gel and other water absorbing components like clay minerals. Fig. 7 shows the distribution of silica gel and water within the inspected sandstone sample. The sample was bonded on a sample holder with an adhesive resulting in absorption maxima at the corners. In this manner, the adhesive on the corners containing hydrogen was taken as a comparison point in the segmentation of the silica gel and adhesive from the rock sample, as seen in Fig. 7.

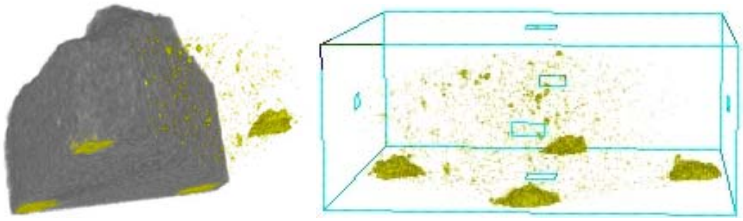

Fig.7: NT images (from 200 projections taken at ATI with 35 seconds per projection) of the silica gel / water distribution within the sandstone; gray segments showing the sandstone and yellow segments silica gel or other hydrogen containing minerals.

3 Conclusions

We presented applications of thermal neutron radiography and tomography in nuclear technology, aerospace and geology/mineralogy. Carrying out the NR experiments at both neutron radiography stations NR II at ATI and NEUTRA at PSI allows showing the effect of the neutron energy spectrum on the attenuation by boron. The measured neutron attenuation coefficients show clear differences after a specific thickness of material, which can be called a detection limit. The good agreement between the experimental and simulated data allows estimating the contribution of the beam hardening and also neutron multiple scattering effects to the radiography image. The micro-inhomogeneities in the material, the beam hardening effect and background strongly influence the attenuation coefficient of a strong absorbing material.

According to the radiographic and tomographic results for fiber reinforced silicon ceramic composites, it can be concluded that the image contrast of the SiC/SiC_f fiber bundles increases with increasing material thickness; the porosity problem exists even in 3 mm thick composites according to the neutron investigations. The measurements showed a one-dimensional fiber bundle-alignment within the SiC/SiC_f composites.

The boron concentration in the TiAl turbine blade is distributed homogeneously up to the detection limit of 300 μm spatial resolution. The heterogeneity increases with the thickness of the TiAl component. Some interior defects like edge cracks could be observed at the transition from thinner to thicker parts, which are probably caused by the manufacturing process.

In the inspections of rock samples, the efficacy of a silica gel impregnation was presented with the help of the strong neutron attenuation property of hydrogen. Besides the visualization of silica gel distribution within the rock samples, water adsorption could be determined with systematic investigations. On this account, the inspections of natural stone based construction material will be continued focusing on the quantitative analysis of water content. The minerals, which contain one of the strong neutron attenuators like H, B, Fe etc., can easily be determined by neutron imaging.

4 Acknowledgement

The authors would like to thank Nikolay Kardjilov for his helps and discussions, Peter Wobrauschek for his helps during the X-ray radiography inspections, Peter Vontobel and Stefan Hartmann for the technical support during the experiments at NEUTRA-PSI. This work was financially supported by the EURATOM-ÖAW, UT4-Underlying Technology project and Böhler Bleche GmbH, Mürzzuschlag.

5 References

[1] M. Bastürk, Material inspections with low energy neutrons and 3D image reconstruction, PhD thesis at TU-Vienna, Austria, 2003.
[2] S. Koerner, Digital image processing in NR, PhD thesis, TU-Vienna 2000.
[3] S. Koerner, B. Schillinger, P. Vontobel, H. Rauch. A neutron tomography facility at a low power research reactor, Nucl. Instr. and Meth. A 471 (2001) 69-74.
[4] A. S. Peréz Ramírez, et al., Tauro:a ceramic composite structural material self-cooled Pb-17Li breeder blanket concept, Journal of Nuclear Materials 233-237 81996) 1257-1261.
[5] L. Giancarli, et al., Design requirements for SiC/SiC composites structural material in fusion power reactor blankets, Fusion Engineering and Design 41 (1998) 165-171.
[6] M. Zawisky , M. Bastürk , J. Rehacek and Z. Hradil, Neutron tomographic investigations of boron-alloyed steels, Journal of Nuclear Materials 327, Issues 2-3, Pages 188-193, 2004.
[7] Report on Böhler NEUTRONIT Boron alloyed steel sheets, Böhler Bleche GmbH (1997).
[8] V.F. Sears, Neutron scattering lengths and cross sections. Neutron News, Vol. 3, No. 3 (1992) p.26.
[9] M. Zawisky, M. Bastürk, R. Derntl, F. Dubus, E. Lehmann, P. Vontobel, Non-destructive ^{10}B Analysis in Neutron Transmission Experiments, Applied Radiation and Isotopes 61 (2004) p. 517.
[10] M. Bastürk, M. Zawisky, N. Kardjilov, E. Lehmann, Radiography investigation and Monte Carlo simulation of neutron transmission through borated steel and aluminum, 7th World Conference on Neutron Radiography, Roma 2002, accepted by IEEE.
[11] M. Zawisky, M. Bastürk, J. Rehacek, Z. Hradil, Neutron tomographic investigations of boron-alloyed steels, Journal of Nuclear Materials 327 (2004) p.188.
[12] S.C. Huang, J.C. Chesnutt, Gamma TiAl and its Alloys, Intermetallic Compounds, vol. 2, John Wiley & Sons, p. 73. 1994.
[13] C.M. Austin, Current status of gamma Ti aluminides for aeurospace applications, Current Opinion in Solid State & Material Science 4, pp. 239-242, 1999.
[14] Donald E. Larsen, Jr., Status of investment cast gamma titanium aluminides in the USA, Material Science & Engineering A213, pp. 128-133, 1996.
[15] T. Tetsui, S. Ono, Endurance and composition and microstructure effects on endurance of TiAl used in turbochargers, Intermetallics 7, pp. 689-697, 1999.
[16] M. H. Loretto et al., The influence of composition and processing on the structure and properties of TiAl-based alloys, Intermetallics 6, pp. 663-666, 1998.
[17] A.-L. Gloanec et al., Fatigue crack growth behaviour of a gamma-titanium-aluminide alloy prepared by casting and powder metallurgy, Scripta Materialia 49, pp. 825-830, 2003.
[18] Steven Weintraub, "Demystifying silica gel, Humidity control with silica gel, silica gel reconditioning", technical papers, Art Preservation Services, **http://www.apsnyc.com/**.